Liquid Crystal Elastomer Balloons

Heidrun Schüring,[†] Ralf Stannarius,*[,†] Christian Tolksdorf,[‡] and Rudolf Zentel*[,‡]

Institut of Experimental Physics I, University of Leipzig, Linnéstrasse 5, D-04103 Leipzig, Germany; and Department of Chemistry, University of Mainz, Duesbergweg 10-14, D-55099 Mainz, Germany.

Received May 16, 2000; Revised Manuscript Received February 25, 2001

ABSTRACT: We describe a setup for mechanical measurements of smectic liquid crystal elastomers and study two materials with different network topologies. The elastic response of macroscopically oriented smectic elastomers to a two-dimensionally isotropic stress in the film plane is measured. The experimental method is based upon the measurement of the inner excess pressure of elastomer balloons, produced by inflation of thin freely suspended films of the smectic material to spherical shape and subsequent photo-cross-linking. We discuss the effects of entropic rubber elasticity and smectic layer compression in the experiment and analyze influences of the network topology (2D or 3D) on the elastic behavior.

Introduction

Liquid crystal (LC) elastomers combine the rubber elasticity of polymer networks with the unique properties of LC phases.[1−5] Because of their broken isotropic orientational symmetry in combination with rubber elasticity, they are promising materials for applications in the field of sensors and actuators. The coupling of mechanical, electrical, and optical properties provides a number of interesting electromechanical as well as optomechanical effects. Although the liquid crystalline phase transitions are nearly unaffected by the network formation, the network retains the memory of the phase and director pattern during cross-linking and establishes a correlation between (macroscopic) mechanical deformations of the material and (microscopic) orientational state of the mesogenic constituents. An attempt to change the director pattern by electric or magnetic fields in LC elastomers leads to a deformation of the network and to an elastic response. As a consequence, nematic LC elastomers could not be switched so far in electric fields, since the dielectric coupling is too weak compared with the elastic forces of the network. For ferroelectric LC, however, the interaction of the spontaneous polarization with the electric field can be considerably larger. It has thus been possible to prepare genuine ferroelectric LC−elastomers.[6−9] The polymer network stabilizes one particular state of mesogen orientation. It acts like an entropy elastic spring which is, however, soft enough to allow a ferroelectric switching of the mesogens. The ferroelectric hysteresis can therefore be measured in these systems. Besides the electrooptical investigations, various experimental methods such as dielectric spectroscopy,[10] Fourier transform IR,[11] AFM,[12] or interferometry[13] have been exploited to study the structure and dynamics of smectic LC−elastomers.

The coupling between the elastic forces of the polymer network and the director reorientation (ferroelectric switching) depends strongly on the network topology (see Figure 1) which can be controlled by a proper choice of the substituents of the starting polymer. If the netpoints are located—preferentially—within the siloxane sublayer (intralayer cross-linking), then the coupling between the director field and elastic network is very weak.[7,14] The network topology is preferentially two-dimensional. It is not possible to stabilize a polar state in the smectic C* phase of these materials. In addition, the switching times are only slightly increased with respect to the non-cross-linked LC polymer. If the cross-links are formed between different siloxane sublayers (interlayer cross-linking, see Figure 1), then the coupling becomes very strong.[6,9−15] In this case the network can stabilize a polar state in the smectic C* phase, ferroelectric switching becomes asymmetric and the switching times do strongly increase. This is shown in Figure 1 for the polymers under investigation in this paper.

Not just the ferroelectric polarization observed in some LC−elastomers distinguishes them from isotropic elastic materials. Also, the mechanical properties of mesogenic elastomers are fundamentally different. For the determination of the elastic moduli of liquid crystalline elastomers, mechanical methods have been proposed.[16,17] A comprehensive review of the elastic properties of LC elastomers can be found in a recent article by Terentjev.[18] One of the novel features predicted by theory is that the rubber−elastic response is in general nonsymmetric, due to the interactions of the anisotropic mesogens with the elastic strain of the network. Another characteristic feature is connected with the layered structure of the smectic phases, which introduces a solidlike elastic response (not directly related with the entropy of the polymer chains) to stresses normal to the layer plane.

Mechanical measurements demonstrating the elastic properties of the cross-linked network have been performed mostly with nematic elastomers.[1−3,19] In the standard experiment, the elastic moduli are determined from a one-dimensional stretching of LC elastomer strips. For elastomers in the smectic A phase, very different moduli have been found for deformations parallel and perpendicular to the smectic layers, respectively.[17] For the switchable ferroelectric networks (chiral smectic C* phase), results are still missing. To understand the influences of network elasticity on the director reorientation (ferroelectric switching) and its relation to mechanical properties in samples with different network topologies, more information on the elastic behavior of the samples is needed.

[†] University of Leipzig.
[‡] University of Mainz.

10.1021/ma000841q CCC: $20.00
Published on Web 05/05/2001

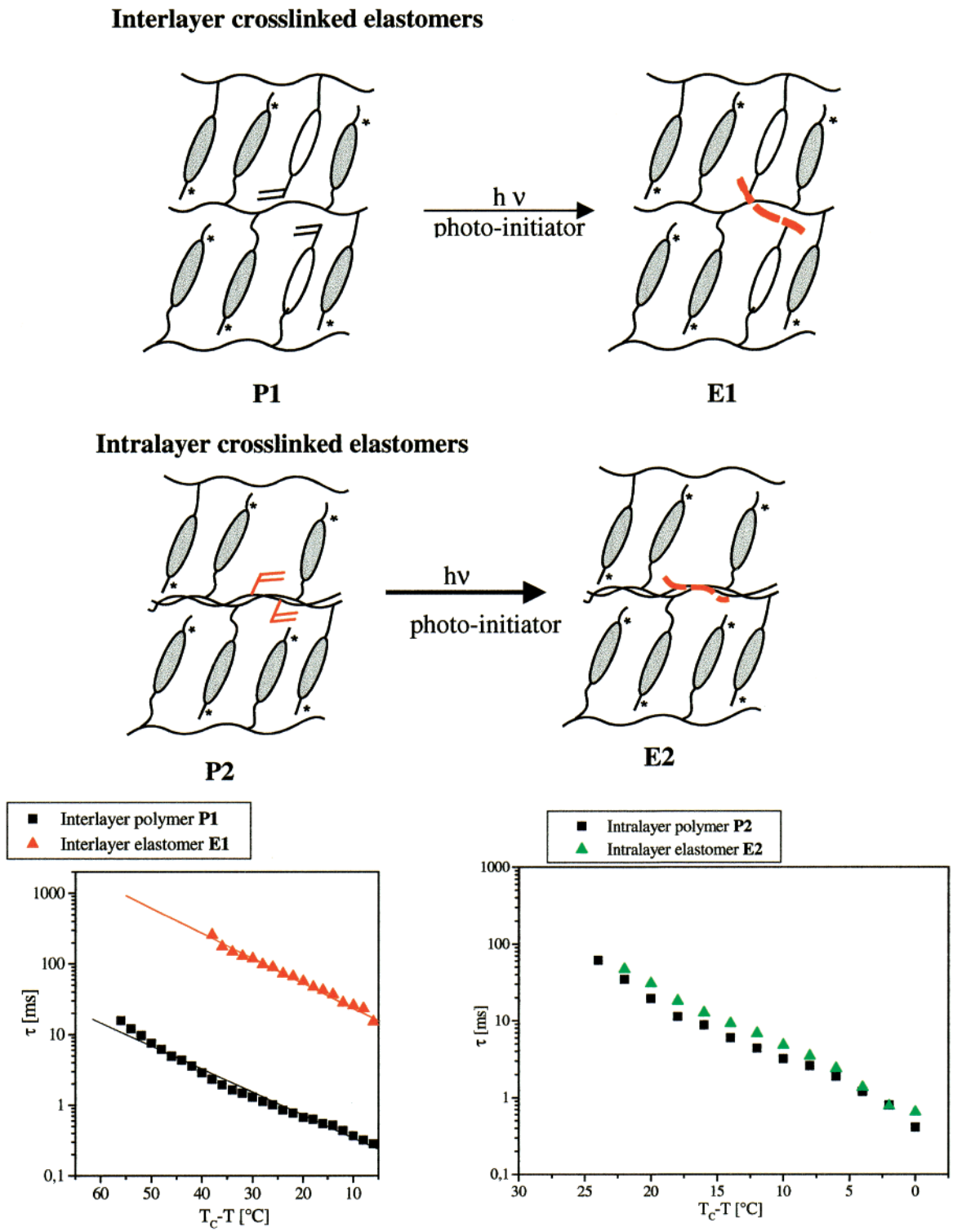

Figure 1. Schematic representation of inter- and intra-cross-linked elastomers (see Schemes 1 and 2 for chemical realization) and their polymer precursors. The lower part shows the effect of cross-linking on the ferroelectric switching times (rise time for 10 μm thick cells, 400 V for **P1** and **E1** or 200 V for **P2** and **E2**, values obtained according to refs 14 and 11 by Tolksdorf and Gebhard for the polymers under investigation).

We have designed an experiment to measure the elastic response of smectic elastomers in macroscopically oriented samples with a simple mechanical setup. The most promising approach to obtain elastic data for these ferroelectric elastomers is the investigation of free-standing smectic films which can be produced in a very efficient way from small amounts of material, and which are characterized by a macroscopic orientational order of the layers.[20] We inflate planar free-standing films of the non-cross-linked material to spherical bubbles by means of a method described earlier[21−23] (similar to the inflation of soap bubbles from planar soap films). The bubbles of several millimeters of diameter are photo-cross-linked to LC−elastomer balloons, which are used for the mechanical experiments described below.

In this paper, we report the synthesis of the two types of ferroelectric LC−elastomers (interlayer and intralayer cross-linked). We introduce their basic character-

Scheme 1. Synthetic Route to the Interlayer Cross-Linkable Polymer P1

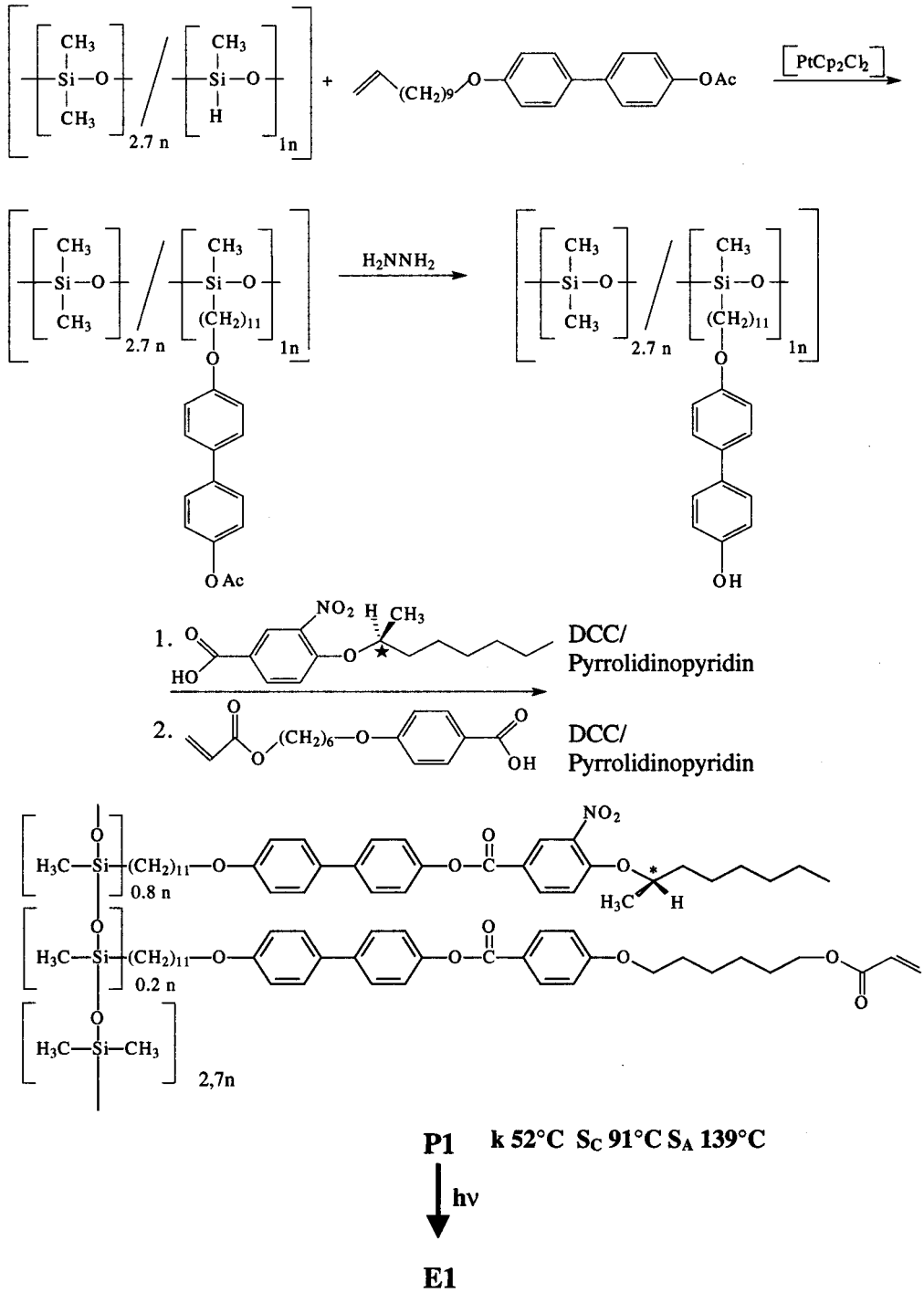

ization and the preparation of LC−elastomer balloons. After the description of the experimental observations, we propose an interpretation of the data and presentation of quantitative evaluation. We discuss the data in the context of a mechanical model and compare the results with those obtained by other groups for different LC elastomer materials.

Experimental Section

Synthesis. The synthesis of the inter- and intra-cross-linkable polymer was done in analogy to known procedures.[6,14,15,24,25] The structure and the synthetic route to the polysiloxane are given in Scheme 1 for the interlayer and in Scheme 2 for the intralayer cross-linked system.

The synthesis of the interlayer polymer **P1** (after cross-linking called **E1**) starts with a classical hydrosilylation of poly(methyl hydrogen-*co*-dimethyl siloxane) (purchased from Wacker) with 4−(undec-10-enyloxy)-4′-acetoxybiphenyl in toluene with $[Pt(C_{10}H_{12})Cl_2$ [26] catalyst (reaction time 3 days). This leads to polysiloxane with a pendent acetate protecting group. Not all Si−H groups could be hydrosilylated with the mesogenic side chain (detected by FT-IR, Si−H at 2160 cm^{-1}). They were removed with a small amount (up to 2 mL) of 1-pentene (the resulting polymers contain, at the most 5% of pentane side groups). After the acetate protecting group was cleaved during a hydrazinolysis in THF/water, the phenolic hydroxy groups could be esterified by a polymer analogous reaction using *N*,*N*′-dicyclohexylcarbodiimid and 4-pyrrolidinopyridin (instead of *N*,*N*′-dimethylaminopyridin due to higher reactivity) in two steps first with 3-nitro-4-(1-(*S*)-methylheptyloxy)benzoic acid (90%) and second with 4-(6-(vinylcarbonyloxy)hexyl)oxybenzoic acid (10%) to obtain the interlayer cross-linkable polymer **P1**. The molar ratio (cross-linkable groups:

Scheme 2. Synthetic Route to the Intralayer Cross-Linkable Polymer P2

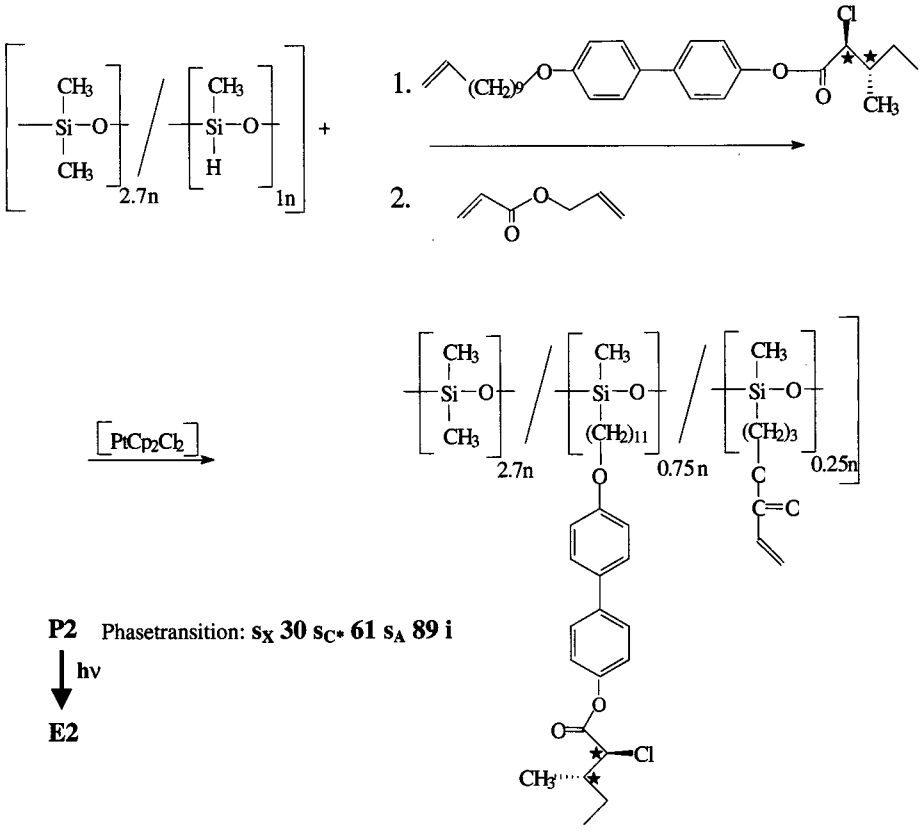

mesogenic groups) was determined by high-resolution ^{1}H NMR.

The intralayer cross-linkable polymer **P2** (after cross-linking called **E2**) was synthesized following the procedures described in the literature.[7] The hydrosilylation of the poly(methyl hydrogen-*co*-dimethyl siloxane) was done in two steps starting with 4′-(10-undecenyloxy)biphenyl-4-yl 2(*S*)-chloro-3-(*S*)-methylpentanoate followed by allyl acrylate (purchased from Lancaster) in toluene with $[Pt(C_{10}H_{12})Cl_2]$ catalyst (molar ratio 9:1; reaction time 3 days). Both polymers were cleaned afterward by precipitation two times from chloroform into methanol. The structures of the polymers were confirmed by IR, ^{1}H NMR and ^{13}C NMR spectroscopy. The phase sequence of **P1** is S_X 52 °C S_C* 91 °C S_A 139 °C iso; for the **P2** polymer, it is S_X 30 °C S_C* 61 °C S_A 89 °C iso.

The phase transition temperatures are determined by DSC, polarization microscopy, X-ray diffraction, and measurements of ferroelectric properties. The results of X-ray measurements are given as Supporting Information. The ferroelectric properties of these types of polymers are discussed in detail in refs 24 and 25. Results measured for the polymers under investigation are given in Schemes 1 and 2.

The polymers were mixed with 1 wt % of 2,4,6-trimethylbenzoyldiphenylphosphine oxide (Lucerin TPO, BASF AG, Ludwigshafen, Germany), a probate photoinitiator for LC polymer films. Irradiation with UV light (preferably about 350 nm) leads to LC−elastomers with qualitatively different physical properties.

Experimental Setup. The basic experimental setup for the preparation of smectic bubbles is similar to that described for the investigation of low molecular weight smectics.[21] Figure 2 shows its principal components. A free-standing film of cross-linkable polymer is drawn on the open end of a glass capillary which is enclosed in a copper thermobox. The temperature in the box can be controlled between room temperature and about 190 °C. At ambient temperature, the viscosity of the polymer is very high, and it is quite impossible to produce free-standing films. Therefore, the material is initially heated, and the films are preferably drawn near the bulk smectic to isotropic transition. Although in general freely suspended films drawn from an isotropic liquid are unstable, films of the LC polymers **P1** and **P2**, can be drawn 5−10 K above the bulk SmA−I phase transition temperature. This is in agreement with the results of Zentel and Decher[20] for planar free-standing films from similar polymers. We attribute this stability to the existence of smectic order at the film surfaces in a certain temperature interval above the bulk clearing point. We inflate the planar film to a bubble by carefully blowing air into the system. The final bubble radius R in the experiments was typically about 3 mm.

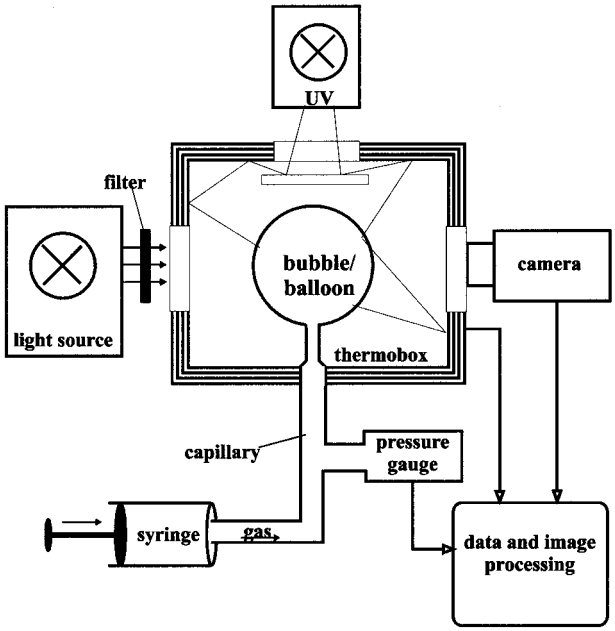

Figure 2. Experimental setup used for the preparation and investigation of LC−elastomer balloons. The capillary diameters are in the range 3−4 mm.

For the optical observation, the bubble is illuminated with parallel light. A filter (borosilicate glass) with a cutoff wavelength of 320 nm is used to prevent uncontrolled photochemical cross-linking. Transmission images are recorded by means of a HAMAMATSU video camera and processed digitally in a computer. The bubble radius can be determined with an accuracy of 0.01 mm with help of image-processing software. In addition to these absolute measurements, a special technique has been applied for the determination of relative radius changes of the elastomer balloons when the inner pressure is varied. Instead of measuring the balloon diameters separately, we use a reference image of the balloon, usually at inner excess pressure close to zero. This reference image is magnified with a proper scaling factor and subtracted digitally from the image that is to be evaluated. When the scaling factor and the position of the reference image are properly chosen, the difference image is uniformly black. This allows us to determine the ratio of the balloon radii with much higher precision than by comparison of data extracted separately from the images. It is also a convenient method to detect potential changes in the balloon shape. If such deviations are observed, this indicates an inhomogeneous cross-linking of the respective balloon and the corresponding data are not included in the further evaluation.

The pressure difference P between the inner of the bubble and the surrounding atmosphere is measured with a very sensitive capacitative pressure gauge (absolute accuracy about 2 Pa, relative accuracy 0.1 Pa). The film thickness is determined optically from the transmission images.[22] The monochromatic light for the film thickness measurements is obtained by metal interference filters with wavelengths in the optical spectrum (430−670 nm). The thickness profiles of the bubbles can be determined with a relative accuracy of about 5% by fitting transmission images for a set of different wavelengths.

For cross-linking, a UV-light source with a radiation intensity of 1500 mW/cm^2 is placed on top of the thermobox, which has been equipped with a quartz-glass window for this purpose (Figure 2). Before UV irradiation, the inflated bubbles are cooled to a temperature in the SmA phase. To ensure uniform cross-linking in all parts of the bubble, it was necessary to block the direct UV beam. The inner surface of the thermobox has been completely covered with randomly reflecting material, which guarantees homogeneous illumination. For the formation of the elastomer network, UV exposure of about 35−60 min is necessary. When cross-linking is finished, material flow from the meniscus into the membrane or within the membrane is prohibited. This can be tested when air is pumped into the system (see details in the next sections).

If, on the other hand, we irradiate the film with the direct UV beam, the dynamics of the cross-linking process in the film is too inhomogeneous. A cap of elastic cross-linked material forms at the most exposed (top) area. It floats, because of small density differences, down the bubble surface, creating strong flow in the surrounding liquid material. Thereby the bubble ruptures or at least becomes strongly inhomogeneous and unusable for further experiments.

General Part

Experimental Observations and Results. For bulk samples, it has been shown that the phase transition temperatures are nearly unaffected (except for a few degrees) by cross-linking.[9] For thin films of these more density cross-linked systems (a factor of 2), careful X-ray measurements are needed to prove this. Temperature-dependent AFM-measurements[12] show smectic layer steps at the surface of similar smectic elastomers even in the isotropic phase. But since the films investigated have a thickness of several hundred layers, we assume that the transitions in the film material, except in thin layers at the air/film interfaces, coincide with the bulk values.

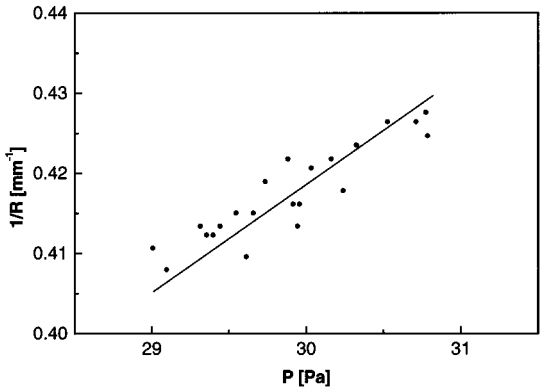

Figure 3. Inverse radius vs pressure characteristics for the un-cross-linked polymer **P2** at a temperature of 73 °C. The straight line is a fit to eq 1 with the slope $(4\sigma)^{-1}$ as the only free parameter; it yields the surface tension $(17.9 \pm 1) \times 10^{-3}$ N/m.

Measurements of the elastic properties have been performed over a broad temperature range to study the dependence of the elastic moduli on temperature and liquid crystalline mesophases. For both materials, the bubbles were cross-linked in the smectic A phase a few kelvin below the bulk SmA−isotropic transition. The smectic phase ranges are very different for the materials **P1** and **P2** (see Schemes 1and 2); this has to be taken into account in the direct comparison of both materials. Before cross-linking, the bubble consists of a layered fluid, and the layer planes are perfectly stacked parallel to the film surface. Within the smectic layers, the material behaves liquidlike without measurable elasticity. The spherical bubble shape is enforced by the minimization of the film surface due to the action of surface tension. The response of the polymer bubble to a change of the air volume inside is completely described by the Laplace-Young relation

$$P = 4\sigma/R \tag{1}$$

where σ is the surface tension and P is the inner excess pressure (Laplace pressure). The factor of 4 accounts for the existence of inner and outer film surfaces. After air is pumped into the bubble, its radius increases whereas the difference pressure decreases and a new equilibrium shape is reached. We note that the surface tension, and consequently the excess pressure P as well, is independent of the film thickness, since no geometrical factor else than the radius of curvature enters eq 1. This has been confirmed experimentally, see also refs 27 and 28. In the experiments, no deviations from the spherical bubble shape have been detected. Figure 3 shows the inner excess pressure as a function of the radius of curvature for the **P2** polymer. Before cross-linking, the polymer bubbles are very sensitive and burst frequently when they are inflated. Therefore, we have refrained from extensive measurements of the $P(R)$ characteristics over a large radius range. It is in principle sufficient to have one datum point for the estimation of σ since the surface tension is the only free fit parameter. The surface tension σ obtained from the pressure and radius data for the intralayer cross-linkable polymer **P2** at 73 °C (S_A), is $(17.9 \pm 1) \times 10^{-3}$ N/m, and for the interlayer cross-linkable polymer **P1** at 137 °C (S_A), it is $(16.8 \pm 1) \times 10^{-3}$ N/m. The $P(R)$ relation is completely determined by surface tension and for the LC polymers σ is in the same range as for low molecular mass smectic materials.[27,28]

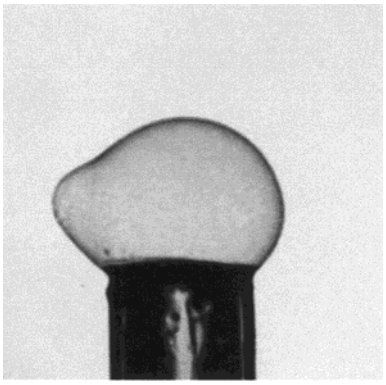

Figure 4. Incompletely cross-linked bubble. Note the pronounced deviation from spherical shape after inflation. The dark structure at the bottom is the capillary.

Technically, it was not possible to observe the bubbles optically during UV exposure, because of the high UV radiation intensity. Through the formation of an elastic network during UV irradiation, the fluidity of the sample vanishes and the viscous and elastic properties of the membrane change dramatically. The first obvious observation is that, in contrast to surface tension controlled bubbles, elastic balloons can exhibit large deviations from spherical shape, if they are cross-linked inhomogeneously. This is reliable evidence that the fluid character of the material is lost. In Figure 4, a balloon with an inhomogeneous thickness profile can be seen. In a part of the sample, cross-linking is not completed. Therefore, the response to a change of the inner gas volume leads to the growth or shrinking of the bump alone whereas the other parts of the membrane remain nearly unaffected. For the quantitative measurements presented below, we have chosen LC balloons which kept their shape during inflation or deflation, ensuring a uniform membrane strain.

When air is blown into a cross-linked bubble, the latter behaves like a rubber balloon, the inner pressure increases as the radius increases. Figure 5 shows the dynamic response of the balloon to a change of inner pressure after the amount of air in the system is changed. In this measurement, the integration time of the pressure sensor was set to 1 s and data are taken every 3 s. Within this resolution the mechanical response to air volume changes is practically undelayed. A detailed dynamic measurement was not intended within this study. For the measurement of the static radius/pressure relation, we wait a few seconds after every pressure change to be sure that the new equilibrium pressure and radius are established. These values remain constant then until the volume of air is changed again. Therefore we can exclude slow relaxations by flow processes of the material in the membrane. The deformations are fully reversible. An experimental test of the reversibility of the strain is the comparison of a balloon at identical parameters before and after temperature and pressure have been varied extensively (see below).

The inner excess pressure can be increased by more than 1 order of magnitude above the initial (Laplace) pressure of the non-cross-linked bubbles, while the balloon size increases only by a few percent. On the other hand, by decreasing the volume of air in the balloon, the pressure difference can be lowered even below zero. This is impossible for bubbles of the un-

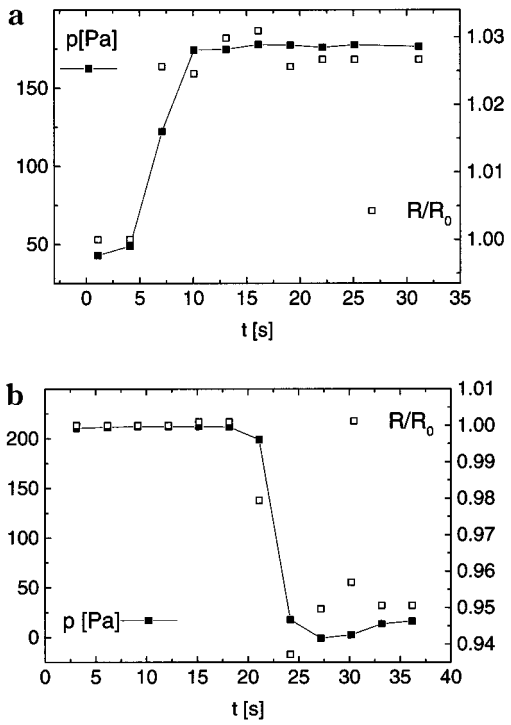

Figure 5. Dynamic behavior of an intralayer bubble after pressure changes at 73 °C: (a) after inflation; (b) after deflation. The radius curve follows the pressure changes without measurable delay.

cross-linked material, since for the purely surface tension controlled polymer a difference pressure $P = 0$ corresponds to a planar film. The membrane area does not shrink below the original size; therefore, the balloons show characteristic crinkles when the volume of air inside is further reduced (Figure 6). After new inflation, the original spherical shape is restored as soon as the difference pressure P becomes positive again.

Figure 7 shows the ratio of the balloon diameter at different temperatures to the diameter at a reference temperature of 48 °C for the **E2** material. After cross-linking the balloon was exposed to temperatures between 40 and 173 °C and the size of the relaxed balloon was determined at different temperatures. The excess pressure was close to zero in these measurements (in the range $0 < P < 6$ Pa, it is difficult to *adjust* an exact pressure difference of zero, although it can be *measured* accurately). Numbers indicate the sequence in which the data points have been taken, the complete sequence was measured over a period of about 2 h. The stability of the balloon in this temperature range gives an additional proof that the elastomer network has completely formed and the liquid fluidity is lost. The temperature characteristics is close to a linear behavior within the experimental error. In particular, no peculiarities of this dependence are indicated at the smectic−isotropic phase transition. When the temperature slope of $\alpha = 0.00028/K$ of the linear fit is interpreted as the linear expansion coefficient of the material, this corresponds to a volume expansion coefficient of about $\gamma = 0.00084/K$. This can be attributed completely to thermal expansion of the mesogenic material, and the expansion coefficient is of the expected magnitude.

The measured pressure characteristics of a balloon of the intralayer cross-linked polymer **E2** is shown in Figure 8 for three different temperatures. Within experimental uncertainty, we can fit the measured rela-

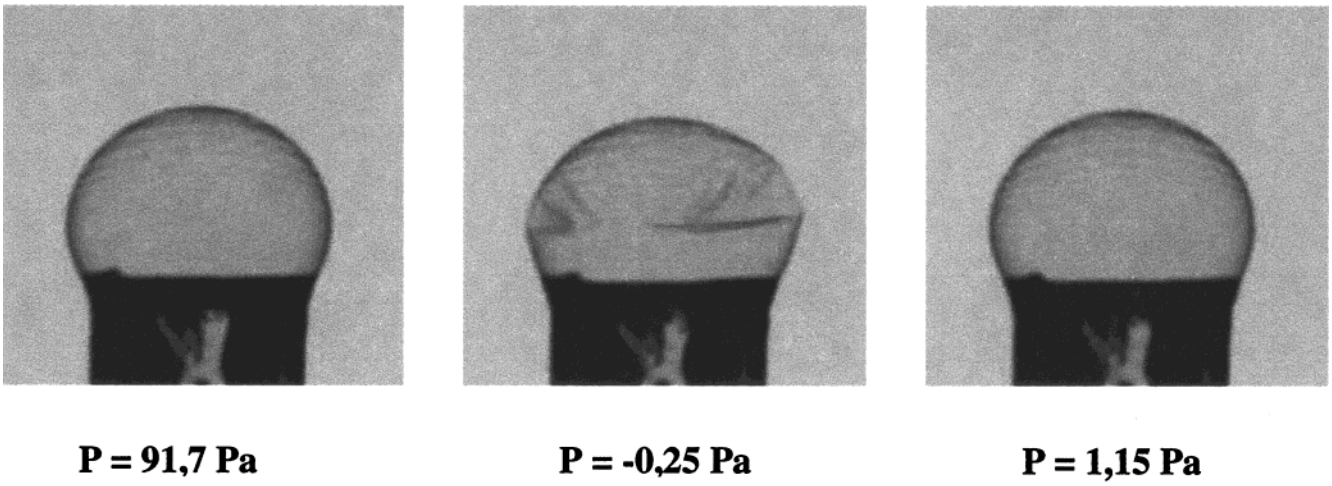

Figure 6. Shape of an LCE balloon (**E2**) at different inner excess pressures. In particular, it is stable at negative difference pressure because of elastic forces. The crinkles are fully reversible. The membrane thickness is 2.3 μm in the middle plane; the diameter is approximately 5 mm.

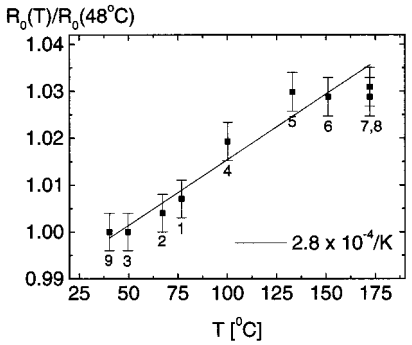

Figure 7. Radius of the relaxed balloon (difference pressure close to zero) as a function of temperature. The radii are determined relative to the radius at 48 °C. The slope gives the linear expansion coefficient of the material. There are no significant indications of anomalies at the smectic−isotropic phase transition. Numbers indicate the sequence in which the data have been measured.

tion between the balloon radius and the inner excess pressure by a linear curve. The slope of these curves is weakly temperature dependent; for lower temperatures, the same excess pressure leads to a larger expansion of the balloon. This slope provides direct access to the elastic properties of the material, and with a suitable model, elastic moduli can be extracted. This is discussed in the next section. The data have been determined with one and the same balloon, so that the film thickness uncertainty does not influence relative changes in the curves. The dotted line in Figure 8a indicates the Laplace pressure (eq 1) of an un-cross-linked polymer bubble with the parameters of the same material.

The temperature dependence of the slope of the $R(P)$ curves is depicted for a second balloon in Figure 9. Again the elasticity of the material decreases with increasing temperature. We find no qualitative differences between data in the smectic and isotropic temperature ranges, which indicates that the same mechanism determines the elastic properties.

The results obtained with different balloons cannot be compared quantitatively before the effects of the different film thicknesses and balloon radii are discussed. On the basis of a model described in the next section, which considers these geometrical differences, the elastic material parameters are determined and compared. We note, however, that the characteristic temperature dependence of the strain vs stress curves presented in Figures 8 and 9 for the individual balloons are model independent. They are not affected by film thickness inhomogeneities which may only be important for an absolute value of the elastic moduli.

A comparison of the interlayer and intralayer LCE balloons reveals qualitatively similar behavior (Figure 10). The interlayer cross-linked sample, which is expected to form a 3-dimensional network, and the intralayer cross-linked material, with a predominantly 2-dimensional network topology, both show comparable characteristics. Both LCE materials show pure elastic response to an isotropic two-dimensional stress in the smectic layer plane. With our setup the maximum achievable expansion of the balloons was about 5%. The applicable pressure was limited: membranes ruptured or the balloons lost contact with the glass capillary and slipped from the support when the inner pressure exceeded about 300 Pa.

Model. Before we analyze the experimental results quantitatively, we give a short qualitative discussion of the observations. Figure 11 illustrates possible scenarios of the R^{-1} vs P characteristics. The solid lines correspond to equilibrium states of a balloon with pure elastic behavior and of a smectic bubble dominated by surface tension, respectively. When the amount of gas in the bubble is changed faster than the characteristic response time of the material, deviations from the curve of equilibrium states are expected as indicated schematically by dashed lines. An inflation or deflation leads to an initial rise or drop, respectively of the inner pressure before the radius changes. Then, the new equilibrium value is approached. In case of a plastic deformation of the cross-linked material, the system would irreversibly leave the initial elastic equilibrium curve (dashed right prolongation of the elastic curve). The shape of the $P(R)$ curve proves to be a sensitive indicator of the viscous, elastic, and plastic characteristics of the cross-linked LC material.

As long as the cross-linking is incomplete, the bubble diameter adapts to the amount of gas inside, and the inner excess pressure relaxes quickly. Only after the material is completely cross-linked, does the increased pressure persist after an inflation and is balanced by the elastic network forces. Our experiments clearly demonstrate that after sufficiently long irradiation the

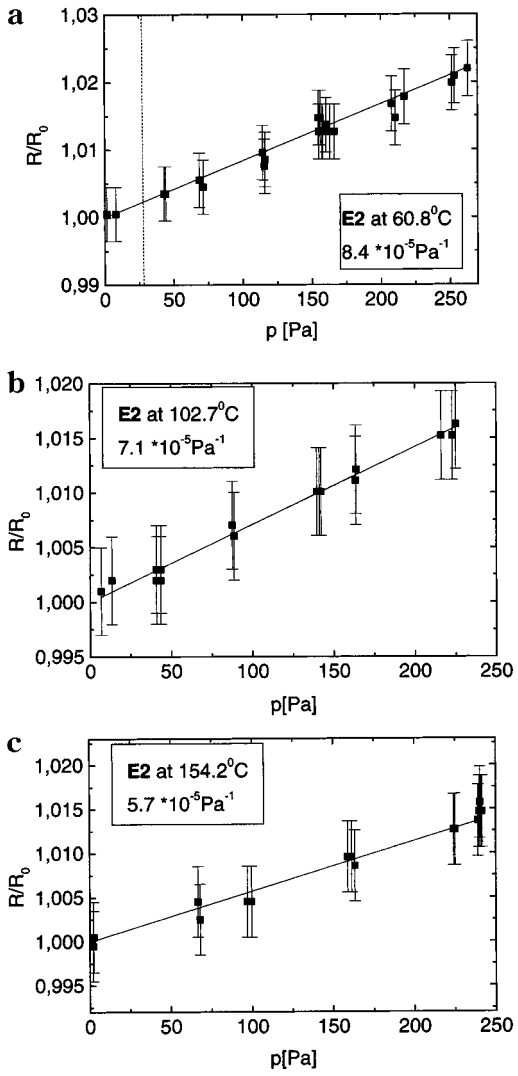

Figure 8. Strain of the elastomer balloon of **E2** as a function of the applied excess pressure at temperatures of (a) 60.8 °C in the smectic C* phase, (b) 102.7 °C, and (c) 154.2 °C in the isotropic phase. The bubble has been inflated at 76 °C and cross-linked at 69 °C. The bubble radius was 2.75 mm; the film thickness increases from 1.65 μm at the top to 3.2 μm at the bottom (2.7 μm in the equatorial plane).

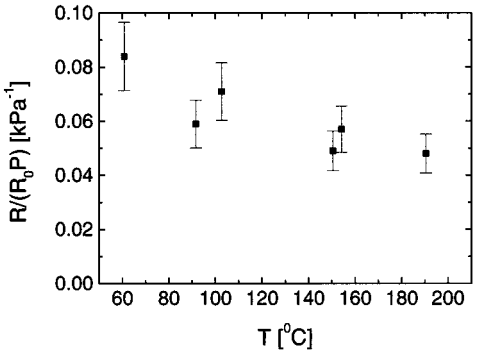

Figure 9. Slopes of the $R(p)$ curves as a function of the temperature, indicating a monotonically increasing elastic modulus with higher temperature: balloon radius 2.27 mm; film thickness in the equatorial plane 3.7 μm (2.4 μm top; 5.0 μm bottom).

samples form LC elastomers, and the material is no longer fluid within the layers. The optimum irradiation time was tested by probing the bubble inflation in regular intervals during irradiation. The necessary

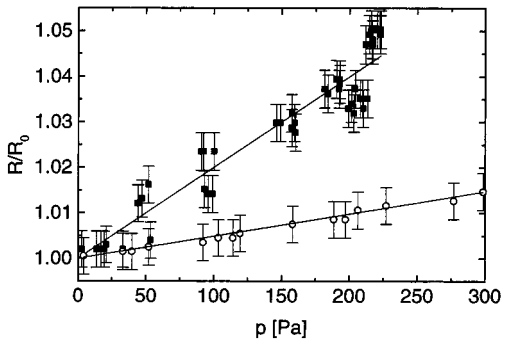

Figure 10. Comparison of intra- (open circles) and interlayer (solid squares) material. The **E1** bubble has been inflated at 139 °C and cross-linked at 125 °C. The elastic data have been measured at 139 °C. The balloon radius was 2.38 mm, and the film thickness in the equatorial plane was 1.80 μm (1.05 μm top; 2.6 μm bottom). For comparison, the graph of the balloon of Figure 8 at 150.15 °C is added. The larger slope of the interlayer material is partially explained by the different film thicknesses but mainly by a smaller elastic modulus.

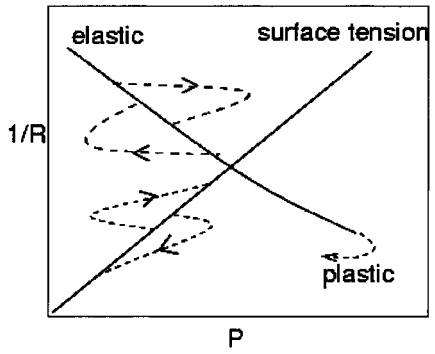

Figure 11. Schematic presentation of the $1/R$ vs P characteristics for small deformations in the case of a pure elastic response and pure surface tension controlled response (solid lines) in equilibrium. The dashed lines symbolize expected nonequilibrium deviations when the pressure changes faster than the viscous response of the bubble, and irreversible (plastic) deformations.

irradiation time depends on the UV intensity, and since we have blocked the direct UV beam and use only the (multiply) reflected light in the chamber, rather long irradiation times arise in our experiment (see sample preparation).

To extract elastic moduli from the experimental data, we have to establish relations between the inner excess pressure (stress) of the balloons and the elastic properties of the membrane (strain). The following calculations apply to a spherical balloon with uniform thickness. We start with the simplest assumption of an isotropic network. In that case, the elastic free energy density f_{el} is given by Mooney's equation[29]

$$f_{el} = C_1(I_1 - 3) + C_2(I_2 - 3) \quad (2)$$

where C_1 and C_2 are material parameters, and I_1 and I_2 are two invariants of the Cauchy strain tensor related to the components λ_x, λ_y, λ_z of the strain by

$$I_1 = \lambda_x^2 + \lambda_y^2 + \lambda_z^2 \quad \text{and}$$
$$I_2 = \lambda_x^2\lambda_y^2 + \lambda_y^2\lambda_z^2 + \lambda_z^2\lambda_x^2 \quad (3)$$

Since the compression modulus C_3 related to the invariant $\lambda_x\lambda_y\lambda_z$ of the Cauchy tensor is independent of the entropy of polymer chain configurations and much

larger than the other two moduli, we can assume incompressibility of the material.

Therefore, we have

$$\lambda_x = \lambda, \quad \lambda_y = \lambda_z = \lambda^{-1/2},$$
$$f_{el} = C_1(\lambda^2 + 2\lambda^{-1}) + C_2(2\lambda + \lambda^{-2}) \quad (4)$$

in the case of a uniaxial stress along x, and

$$\lambda_x = \lambda_y = \lambda, \quad \lambda_z = \lambda^{-2},$$
$$f_{el} = C_1(2\lambda^2 + \lambda^{-4}) + C_2(\lambda^4 + 2\lambda^{-2}) \quad (5)$$

for isotropic stress in the xy plane. The relation between C_1, C_2, and the excess pressure P in the balloon can be found by equating the free elastic deformation energy $dF_{el} = V_f\, df_{el}$ to the work $p\, dV$ done by the gas in the balloon. Here $V_f = 4\pi R^2 D = 4\pi {R_0}^2 D_0$ is the volume of the elastomer film, D is the film thickness, D_0 the initial value of D and R_0 the initial value of R, where $D_0 \ll R_0$. Combining $\lambda = R/R_0$, $dV = 4\pi R^2\, dR$, and eq 5, we find

$$p = \frac{dF_{el}}{dV} = \frac{1}{4\pi R^2}\frac{d}{dR}4\pi {R_0}^2 D_0\left[C_1\left(2\frac{R^2}{{R_0}^2} + \frac{{R_0}^4}{R^4}\right) + C_2\left(\frac{R^4}{{R_0}^4} + 2\frac{{R_0}^2}{R^2}\right)\right] = \frac{4D_0}{R_0}\left[C_1\left(\frac{R_0}{R} - \frac{{R_0}^7}{R^7}\right) + C_2\left(\frac{R}{R_0} - \frac{{R_0}^5}{R^5}\right)\right] \quad (6)$$

for small deformations $\delta R = R - R_0 \ll R_0$ of the bubble, we can simplify this equation to

$$p = \frac{4D_0}{R_0}6(C_1 + C_2)\frac{\delta R}{R_0} \quad (7)$$

In a smectic elastomer, one has to consider an additional free energy contribution of the form

$$f_{sm} = \frac{1}{2}B\left(\frac{du}{dz}\right)^2 \quad (8)$$

where u is the layer displacement and z is the coordinate normal to the smectic film surface. It describes the elastic compression of the smectic layer. Nishikawa et al.[17] have found for some elastomers in the smectic A phase that the layer compression modulus B can be orders of magnitude larger than the rubber elastic moduli. Consequently, when a uniaxial stress is applied to such smectic A free-standing films in the layer plane, the layers (in the xy plane) can be considered unchanged and $\lambda_z = 1$, while $\lambda_x = \lambda = \lambda_y^{-1}$. Figure 12 sketches the deformation of a smectic A film under the action of uniaxial stress in the layer plane. The in-plane contraction perpendicular to the stress axis compensates the strain along the stress axis, the layer thickness is practically unchanged. Then, eq 4 leads to

$$p = \frac{dF_{el}}{dV} = \frac{2y_0z_0}{yz}(C_1 + C_2)\left(\frac{x}{x_0} - \frac{{x_0}^3}{x^3}\right) \quad (9)$$

and for small δx in linear approximation

$$p = 8(C_1 + C_2)\frac{\delta x}{x_0} \quad (10)$$

In the case of in-plane isotropic stress, the material

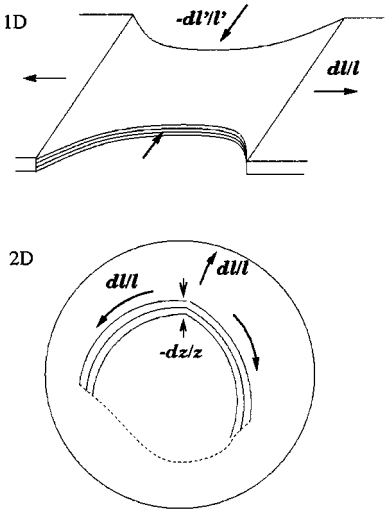

Figure 12. Schematic sketch of uniaxial (1D) stretching of a planar free-standing LC−elastomer film and the in-plane isotropic (2D) stretching of the elastomer bubble.

cannot respond with a lateral contraction in the layer plane and the system should contract normal to the layer. The corresponding strain components are $\lambda_x = \lambda_y = \lambda = R/R_0$, $\lambda_z = \lambda^{-2}$. The elastic contribution of the layer compression modulus is found from eq 8. The layer displacement u is related to the normal strain by

$$u = (\lambda_z - 1)z = (\lambda^{-2} - 1)z \quad (11)$$

Therefore we have

$$F_{sm} = 4\pi R^2 D\frac{1}{2}B\left(\frac{{R_0}^2}{R^2} - 1\right)^2$$

and

$$p = \frac{dF_{sm}}{dV} = \frac{{R_0}^2 D_0}{2R^2}B\frac{d}{dR}\left(\frac{{R_0}^2}{R^2} - 1\right)^2 = \frac{2D_0}{R}B\left(\frac{{R_0}^4}{R^4} - \frac{{R_0}^6}{R^6}\right) \quad (12)$$

In the limit of small (positive) deformations, δR, the equation can be reduced to

$$p = 4D_0B\left(\frac{1}{R_0} - \frac{1}{R}\right) \quad \text{or} \quad p = \frac{4D_0}{R_0}B\frac{\delta R}{R_0} \quad (13)$$

The relaxed radius R_0 is reached in the limit $p = 0$, and the slope of the radius vs pressure curve (in absence of entropy elasticity for small deformations) is linearly related to the elastic compression modulus. As in eq 7, the excess pressure in the balloon is directly proportional to the film thickness D_0 which has to be determined by appropriate optical methods.

In the last paragraph, we have assumed that the smectic layers are compressed when the material is stretched isotropically in the plane. Of course, the film has other alternatives to retain its volume under lateral strain. The first one, a reduction of the number of smectic layers, should be clearly identified from the experiment. Such a process, equivalent to the partial rupture of the film, would be irreversible, in contrast to the experimental observations. Another alternative is the tilt of the molecular axes with respect to the layer

normal. With such an induced tilt (like in an induced SmA to SmC transition) the layer thickness would decrease with increasing tilt angle. Thus, the system could also respond to lateral stress with an induced tilt.

Discussion

The preceding models are based on a number of assumptions which have to be checked carefully when the models are applied to experimental data. For example, entropy elasticity and layer compression can appear in combination. Furthermore, the assumption of a complete spherical membrane is not exact since the balloons sit on a rigid capillary opening. Finally, a uniform membrane thickness has not been achieved so far in the experimental balloons. Nevertheless, data obtained with one and the same balloon can be directly compared to obtain information on the thermal characteristics of the elasticity. The determination of absolute elastic coefficients yields reproducible results which are correct within about 25% uncertainty.

The film thickness of the polymer bubbles (in contrast to low molecular weight materials) is generally nonuniform. The time to achieve a uniform thickness after inflation of the sphere is too large for practical experiments. Usually a considerable thickness gradient from top to bottom is found. This thickness gradient turns out to be the largest error source in the exact quantitative calculation of the elastic modulus. The relations derived in the previous section are only a first approximation for the observed balloons where the film thickness can change by about 50% from top to bottom.

On the basis of the models presented in the previous section, the experimental data can be interpreted in the following way.

The most striking result is the fact that there is no qualitative change of the stress/strain relation at the transition from the smectic to the isotropic phase of the materials, although we would expect pure rubber elastic behavior in the isotropic range and an additional smectic layer compression effect in the smectic phase only. Even if we assume small changes of the phase transition temperatures in the deformed thin membranes, this will not explain the observations. For example, the temperature range covered by the experiment extends more than 100 K above the smectic mesophase in **E2**. The point that the layer compression effect is not reflected by the elastic data may be a result of the high cross-linking density: the high entropy elasticity masks its contribution. Since in the isotropic phase, the layer compression effect is absent, we can interpret at least the high temperature measurements completely in terms of a rubber elastic theory. We introduce the elastic modulus $E = 6(C_1 + C_2)$ which can be directly extracted from the slope of the radius/pressure characteristics. Figure 13 shows the elastic modulus obtained from the linear fit of radius vs pressure curves for the two elastomer materials. The open and solid circles and squares represent data obtained from three different balloons of the intralayer cross-linked elastomer **E2**. While the radius data are exact, we have used the average thickness of the membrane for each balloon, which is only an rough approximation. None of the balloons had a homogeneous film thickness. On a molecular level, the film thickness inhomogeneity is small, on average a one layer step occurs every 50 μm, so the role of defects in the layer structure in the smectic phases should still be negligible.

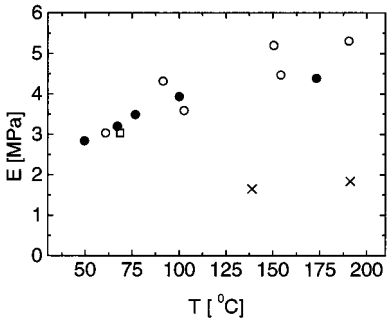

Figure 13. Comparison of elastic moduli obtained from different balloons. Key: crosses, interlayer elastomer **E1**, bubble diameter and film thickness as in Figure 10; open circle, **E2**, parameters of Figure 8; solid circles, **E2**, parameters of Figure 9; open box, **E2**, $R_0 = 2.33$ mm, $D_0 = 3.2$ μm in the equator (1.92 μm top, 4.5 μm bottom).

However, the inhomogeneity will lead to different strains of the top and bottom hemispheres of the balloons and a change of their shape. Since the strains are small in our experiments, we have not been able to detect such shape distortions. For an improvement of the absolute accuracy of the elastic moduli data it will be necessary to find preparation techniques for uniform balloons. Another approximation in the evaluation of the data with our model is the assumption of completely spherical balloons. Since the balloon is supported on a capillary and the capillary radius of about 1.8 mm is not small compared to the balloon size, the actual deformation would not be uniform even in the case of a uniform membrane. The calculation of the corrected deformation is not possible analytically; therefore, the solution will be the study of balloons with radii much larger than that of the capillary, which have not been achieved yet. The influence of this approximation on the comparison of data of different balloons is negligible because the ratios of capillary to balloon radii were approximately the same for all balloons investigated, but probably a small systematic correction of the absolute elastic moduli is the consequence.

The basic conclusion of Figure 13 is that, within the model, we find a good quantitative agreement between the data obtained from different balloons, the temperature characteristics $dE/dT > 0$ are undoubtedly established for the intralayer material, and quantitative data for the elastic moduli have been determined. For the interlayer material **E1** (crosses), the elastic modulus is significantly smaller than for the intralayer elastomer. From the chemical point of view this is the result of the smaller volume density of cross-linkable groups in **P1**, as the large mesogenic groups between polymer chain and cross-linkable groups are missing (the molar mass per cross-linkable group is larger in **P1** than in **P2**). A temperature characteristics has not been established yet for this compound, but the data are consistent with a positive temperature slope, too.

Since we do not find a significant difference in the elastic properties between the isotropic and smectic ranges, we conclude that the elastic behavior is completely controlled by the rubber elastic modulus in these balloons. The relatively large cross-linking density is responsible for the dominant entropy elasticity. If we are interested in the study of the influence of the smectic layer compression effects, it seems that the amount of cross-linker groups has to be reduced considerably.

Summary and Outlook

We have developed a method for the preparation of elastomer balloons from self-supporting smectic bubbles. These balloons consist of LC elastomers which are macroscopically aligned due to the preparation technique, the smectic layers are stacked within the film plane. The method described allows the investigation of elastic properties of these materials. From the measurement of the radius vs pressure characteristics, we can determine qualitatively the change from surface tension controlled liquid crystalline behavior to elastic behavior of the cross-linked material after UV irradiation. It has been verified that after cross-linking the network prevents flow in the smectic membranes. The radius vs pressure curves also provide a quantitative measure for the elastic data. We have presented models for the influences of rubber elastic properties and smectic layer compression on the radius-pressure characteristics. In the balloons studied here, the entropy elastic modulus is dominant, and the balloons exhibit typical rubber elastic properties. An influence of different mesophases is not detected.

In view of the fact that, for the two materials with different network topologies, considerable qualitative differences in electrooptic behavior have been found, it is interesting that the elastic properties of the network are rather similar. Irrespective of the factor of about 2 in the elastic moduli derived from the experiments, the elastic behavior in the balloon experiments is qualitatively the same.

It should also be noted that we do not find a change of the balloon dimensions at the phase transitions of the mesogenic material. In nematic elastomers, huge thermoelastic changes in the macroscopic sample dimensions at the isotropic phase transition can be observed as a consequence of the coupling of molecular orientational order to the elastic network.[30] In our samples, the cross-linking density is obviously too large to observe such an effect.

Finally, we give some outlook for future experiments which are being performed to underpin some predictions of our model. The cross-linking density has to be modified to access the layer compression or induced tilt effects in the smectic mesophases. Moreover, experimental improvements have to be achieved. The preparation of balloons of uniform thickness, which have much larger radii than the capillary opening, will be the precondition for an improvement of quantitative data. Achievement of a good contact of the balloon at the capillaries, by selection of proper surfaces, will increase the available pressure and strain range. Furthermore, X-ray and long-range polarizing microscope measurements in the thin balloon membranes are in preparation to study structure details.

Acknowledgment. This work was supported within Sonderforschungsbereich 294 (Leipzig) and a DFG grant (Mainz). The authors acknowledge discussions with F. Kremer.

Supporting Information Available: Text and figures showing X-ray measurements for phase assignment of uncross-linked and cross-linked polymers. This material is available free of charge via the Internet at http://pubs.acs.org.

References and Notes

(1) Zentel, R. *Angew. Chem. Adv. Mater.* **1989**, *101*, 1437.
(2) Gleim, W.; Finkelmann, H. In *Side Chain Liquid Crystalline Polymers*; McArdle, C. B., Ed.; Blackie and Son: Glasgow, Scotland, 1989, p 287.
(3) Finkelmann, H. In *Liquid Crystallinity in Polymers*; Ciferri, A., Ed.; VCH: Weinheim, Germany, 1991, p 315.
(4) Davis, F. J. *J. Mater. Chem.* **1993**, *3*, 551.
(5) Brehmer, M.; Zentel, R. *Mol. Cryst. Liq. Cryst.* **1994**, *243*, 353.
(6) Brehmer, M.; Zentel, R.; Wagenblast, G.; Siemensmeyer, K. *Macromol. Chem. Phys.* **1994**, *195*, 1891.
(7) Brehmer, M.; Zentel, R. *Macromol. Chem. Rapid Commun.* **1995**, *16*, 659.
(8) Benné, I.; Semmler, K.; Finkelmann, H. *Macromolecules* **1995**, *28*, 245.
(9) Brehmer, M.; Zentel, R.; Giesselmann, F.; Germer, R.; Zugenmaier, P. *Liq. Cryst.* **1996**, *21*, 589.
(10) Gebhard, E.; Zentel, R. *Liq. Cryst.* **1999**, *26*, 299.
(11) Shilov, S. V.; Skupin, H.; Kremer, F.; Gebhard, E.; Zentel, R. *Liq. Cryst.* **1997**, *22*, 203. Skupin, H.; Kremer, F.; Shilov, S. V.; Lehmann, W.; Brodowsky, H. M.; Gebhard, E.; Zentel, R. *J. Macromol. Sci.—Phys. B* **1999**, *38*, 709.
(12) Brodowsky, H. M.; Boehnke, U.-C.; Kremer, F.; Gebhard, E.; Zentel, R. *Langmuir* **1999**, *15*, 274.
(13) Lehmann, W.; Gattinger, P.; Keck, M.; Kremer, F.; Stein, P.; Eckert, T.; Finkelmann, H. *Ferroelectrics* **1998**, *208—209*, 373.
(14) Gebhard, E.; Zentel, R. *Macromol. Chem. Phys.* **2000**, *201*, 902.
(15) Gebhard, E.; Zentel, R. *Macromol. Chem. Phys.* **2000**, *201*, 911.
(16) Kundler, I.; Nishikawa, E.; Finkelmann, H. *Macromol. Symp.* **1997**, *117*, 11.
(17) Nishikawa, E.; Finkelmann, H.; Brand, H. R. *Macromol. Rapid Commun.* **1997**, *18*, 65. Nishikawa, E. Dissertation, Freiburg, Germany, 1997.
(18) Terentjev, E. M. *J. Phys. Condens. Matter* **1999**, *11*, R239.
(19) Küpfer, J.; Finkelmann, H. *Makromol. Chem. Rapid Commun.* **1991**, *12*, 717.
(20) Reibel, J.; Brehmer, M.; Zentel, R.; Decher, G. *Adv. Mater.* **1995**, *7*, 849.
(21) Stannarius, R.; Cramer, C. *Europhys. Lett.* **1998**, *42*, 43.
(22) Stannarius, R.; Cramer, C.; Schüring, H. *Mol. Cryst. Liq. Cryst.* **1999**, *339*, 1035.
(23) Oswald, P. *J. Phys.* **1987**, *48*, 897.
(24) Poths, H.; Zentel, R. *Liq. Cryst.* **1994**, *16*, 749.
(25) Kapitza, H.; Zentel, R.; Twieg, R. J.; Nguyen, C.; Vallerien, S. U.; Kremer, F.; Wilson, C. G. *Adv. Mater.* **1990**, *4*, 792.
(26) Apfel, M. A.; Finkelmann, H.; Janini, G. M.; Laub, R. J.; Lühmann, B.-H.; Prive, A.; Roberts, W. L.; Shaw, T. J.; Smith, C. A. *Anal. Chem.* **1985**, *57*, 651.
(27) Schüring, H.; Thieme, C.; Stannarius, R. *Liq. Cryst.* **2001**, *28*, 241.
(28) Mach, P.; Huang, C. C.; Stoebe, T.; Wedell, E. D.; Nguyen, T.; de Jeu, W. H.; Guittard, F.; Naciri, J.; Shashidhar, R.; Clark, N.; Jiang, I. M.; Kao, F. J.; Liu, H.; Nohira, H. *Langmuir* **1998**, *14*, 4330.
(29) See, e.g.: Batzer, H., Ed. *Polymere Werkstoffe*; Thieme: Stuttgart, Germany, 1985; Vol. I.
(30) de Gennes, P.; Hébert, M.; Kant, R. *Macromol. Symp.* **1997**, *113*, 39.

MA000841Q